Fourier finite-difference wave propagation[a]

[a]Published in Geophysics, 76, T123-T129, (2011)

Xiaolei Song and Sergey Fomel

ABSTRACT

We introduce a novel technique for seismic wave extrapolation in time. The technique involves cascading a Fourier Transform operator and a finite difference operator to form a chain operator: Fourier Finite Differences (FFD). We derive the FFD operator from a pseudo-analytical solution of the acoustic wave equation. 2-D synthetic examples demonstrate that the FFD operator can have high accuracy and stability in complex velocity media. Applying the FFD method to the anisotropic case overcomes some disadvantages of other methods, such as the coupling of qP-waves and qSV-waves. The FFD method can be applied to enhance accuracy and stability of seismic imaging by reverse-time migration.

INTRODUCTION

The wavefield extrapolation problem refers to advancement of a wavefield through space or time. Both extrapolation in depth and extrapolation in time can be used in seismic modeling and seismic migration. Reverse time migration, or RTM (Baysal et al., 1983; McMechan, 1983; Whitmore, 1983; Levin, 1984), involves wave extrapolation forward and backward in time. RTM is useful for accurate imaging in complex areas and is drawing more and more attention as the most powerful depth-imaging method (Yoon et al., 2004; Symes, 2007; Fletcher et al., 2009; Fowler et al., 2010).

Reverse-time migration can correctly handle complex velocity models without dip limitations on the image. However, it has large memory requirements and needs a significant amount of computation. The most popular and straightforward way to implement reverse-time migration is the method of explicit finite differences, which is only conditionally stable because of the limit on time-step size. Finite-difference methods also suffer from numerical dispersion problems, which can be overcome either by decreasing the time step or by high-order schemes (Wu et al., 1996; Liu and Sen, 2009). Several alternative algorithms have been developed for seismic wave extrapolation in variable velocity media. Soubaras and Zhang (2008) introduced an algorithm based on a high-order differential operator, which allows a large extrapolation time step by solving a coefficient optimization problem. Zhang and Zhang (2009) proposed one-step extrapolation method by introducing a square-root operator. This method can formulate the two-way wave equation as a first-order partial differential equation

in time similar to the one-way wave equation. Etgen and Brandsberg-Dahl (2009) modified the Fourier Transform of the Laplacian operator to compensate exactly for the error resulting from the second-order time marching scheme used in conventional pseudo spectral methods (Reshef et al., 1988a). Fowler et al. (2010) provided an accurate VTI P-wave modeling method with coupled second-order pseudo-acoustic equations. Pestana and Stoffa (2010) presented an application of Rapid Expansion Method (REM) (Tal-Ezer et al., 1987) for forward modeling with one-step time evolution algorithm and RTM with recursive time stepping algorithm.

In this paper, we present a new wave extrapolator derived from the pseudo-analytical approach of Etgen and Brandsberg-Dahl (2009). Our method combines FFT and finite differences. We call it the Fourier Finite Difference method because it is analogous to the concept introduced previously for one-way wave extrapolation by Ristow and Ruhl (1994).

As a chain operator of Fast Fourier Transform and Finite Difference operators, the proposed extrapolator can be as accurate as the parameter interpolation approach employed by Etgen and Brandsberg-Dahl (2009) but at a cost of only one Fast Fourier Transform (FFT) and inverse Fast Fourier Transform (IFFT) operation. The advantages of the FFD operator are even more apparent in the anisotropic case: no need for several interpolations for different parameters with the corresponding computational burden of several FFTs and IFFTs. In addition, the operator can overcome the coupling of qP-waves and qSV-waves (Zhang et al., 2009). We demonstrate the method on synthetic examples and propose to incorporate FFD into reverse-time migration in order to enhance migration accuracy and stability.

THEORY

The acoustic wave equation is widely used in forward seismic modeling and reverse-time migration (Bednar, 2005; Etgen et al., 2009):

$$\frac{\partial^2 p}{\partial t^2} = v(\mathbf{x})^2 \, \nabla^2 p \; , \tag{1}$$

where $p(\mathbf{x}, t)$ is the seismic pressure wavefield, and $v(\mathbf{x})$ is the propagation velocity. Assuming a constant velocity v, after Fourier transform in space, we can get the following explicit expression:

$$\frac{d^2 \hat{p}}{dt^2} = -v^2 |\mathbf{k}|^2 \hat{p} \; , \tag{2}$$

where

$$\hat{p}(\mathbf{k}, t) = \int_{-\infty}^{+\infty} p(\mathbf{x}, t) e^{i\mathbf{k}\cdot\mathbf{x}} d\mathbf{x} \; . \tag{3}$$

Equation 2 has the following solution:

$$\hat{p}(\mathbf{k}, t + \Delta t) = e^{\pm i |\mathbf{k}| v \Delta t} \hat{p}(\mathbf{k}, t) \; . \tag{4}$$

A second-order time-marching scheme and the inverse Fourier transform lead to the well-known expression (Etgen, 1989; Soubaras and Zhang, 2008):

$$p(\mathbf{x},t+\Delta t)+p(\mathbf{x},t-\Delta t)-2p(\mathbf{x},t) = \\ 2\int_{-\infty}^{+\infty}\hat{p}(\mathbf{k},t)(\cos(|\mathbf{k}|v\Delta t)-1)e^{-i\mathbf{k}\cdot\mathbf{x}}d\mathbf{k}\ . \tag{5}$$

Equation 5 provides an elegant and efficient solution in the case of a constant-velocity medium with the aid of FFT. In the case of a variable-velocity medium, equation 5 can provide an approximation by replacing v with $v(\mathbf{x})$. However, FFT can no longer be applied directly for the inverse Fourier transform from the wavenumber domain back to the space domain. To overcome this problem, Etgen and Brandsberg-Dahl (2009) propose a velocity interpolation method. They present an implementation for isotropic, VTI (vertical transversely isotropic) and TTI (tilted transversely isotropic) media. In the isotropic case, two FFTs can be sufficient. For anisotropic media, more than one velocity parameter must be used. Therefore, it is necessary to perform velocity interpolation by combining different parameters and computing the corresponding forward and inverse FFTs for each of the velocity parameters, thus increasing the computational burden. Other FFT-based solutions include the optimized separable approximation or OSA (Song, 2001; Liu et al., 2009; Zhang and Zhang, 2009; Du et al., 2010) and the lowrank approximation (Fomel et al., 2010).

We propose an alternative approach. First, we adopt the following form of the right-hand side of equation 5 in the variable velocity case:

$$2\left[\cos(v(\mathbf{x})|\mathbf{k}|\Delta t)-1\right] = \\ 2\left[\cos(v_0|\mathbf{k}|\Delta t)-1\right]\left[\frac{\cos(v(\mathbf{x})|\mathbf{k}|\Delta t)-1}{\cos(v_0|\mathbf{k}|\Delta t)-1}\right]\ , \tag{6}$$

where v_0 is the reference velocity, such as the RMS (root-mean-square) velocity of the medium. After that, we apply the following approximation:

$$\frac{\cos(v(\mathbf{x})|\mathbf{k}|\Delta t)-1}{\cos(v_0|\mathbf{k}|\Delta t)-1}\approx a+2\sum_{n=1}^{3}b_n\cos(k_n\Delta x_n)\ , \tag{7}$$

where coefficients a and b_n are defined using the Taylor expansion around $k=0$,

$$a=\frac{v^2(\mathbf{x})}{v_0^2}\left[1+\frac{(\Delta t)^2(v_0^2-v^2(\mathbf{x}))(\Delta x_1^2\Delta x_2^2+\Delta x_2^2\Delta x_3^2+\Delta x_3^2\Delta x_1^2)}{6\Delta x_1^2\Delta x_2^2\Delta x_3^2}\right] \\ b_n=\frac{(\Delta t)^2v^2(\mathbf{x})(v^2(\mathbf{x})-v_0^2)}{12(\Delta x_n^2)v_0^2}\ , \tag{8}$$

and Δx_n is the sampling in the n-th direction. We only need to calculate these coefficients once. After completing the calculation, they can be used at each time step during the wave extrapolation process.

Equation 6 consists of two terms: the first term is independent of $\mathbf{x}$ and only depends on $\mathbf{k}$. For this part, we use inverse FFT to return to the space domain from the

wavenumber domain. For the remaining part, however, we can avoid phase shift in the wavenumber domain by implementing space shifts through finite differences (approximation 7) with coefficients provided by equation 8. This approach is analogous to the FFD method proposed by Ristow and Ruhl (1994) for one-way extrapolation in depth.

Figure 1 (a) shows approximations for $[\cos(v(\mathbf{x})|\mathbf{k}|\Delta t) - 1]$ by the 4th-order FD method (dash line) and pseudo-spectral method (dotted line). Figure 1 (b) shows approximations by the FFD method (2nd-order: dash line, 4th-order: dotted line). The solid lines stand for the exact values for function $[\cos(v(\mathbf{x})|\mathbf{k}|\Delta t) - 1]$ with true velocity: $v = 4.0km/s$ (bottom solid line) and $v_0 = 2.0km/s$ (top solid line), which indicates a significant velocity contrast (100% difference). In this situation, all the approximations deviate from the exact solution as the wavenumber $|k|$ becomes large. However, the 4th-order FFD method approximates the exact solution with the most accuracy, as shown in the error plot (Figure 2). In order to enhance the stability, one can suppress the wavefield at high wavenumbers for both pseudo-spectral and the FFD method.

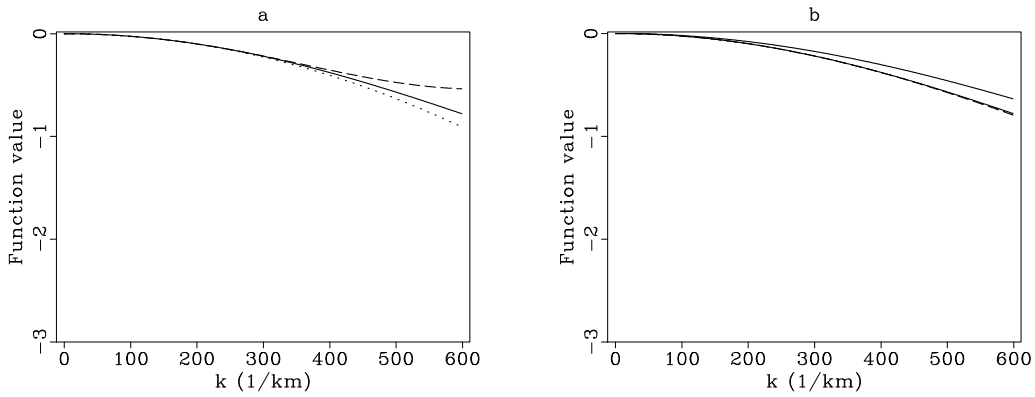

Figure 1: Different approximations for $\cos(v(\mathbf{x})|\mathbf{k}|\Delta t) - 1$. Solid lines: exact solution $(\cos(v(\mathbf{x})|\mathbf{k}|\Delta t) - 1)$ for $v = 4.0$ km/s and $v_0 = 2.0$ km/s. (a) Dash line: the 4th-order FD. Dotted line: pseudo-spectral method. (b) Dash line: the 2nd-order FFD method. Dotted line: the 4th-order FFD with v_0 as reference velocity. $\Delta t = 0.001$ s. $\Delta x = 0.005\, km$.

Assuming that $p(\mathbf{x}, t - \Delta t)$ and $p(\mathbf{x}, t)$ are already known, the time-marching algorithm can be specified as follows:

1. Transform $p(\mathbf{x}, t)$ to $\hat{p}(\mathbf{k}, t)$ by 3-D FFT;
2. Multiply $\hat{p}(\mathbf{k}, t)$ by $2\,[\cos(v_0|\mathbf{k}|\Delta t) - 1]$ to get $\hat{q}(\mathbf{k}, t)$;
3. Transform $\hat{q}(\mathbf{k}, t)$ to $q(\mathbf{x}, t)$ by inverse FFT;
4. Apply finite differences to $q(\mathbf{x}, t)$ with coefficients in equation 8 to get $q(\mathbf{x}, t +$

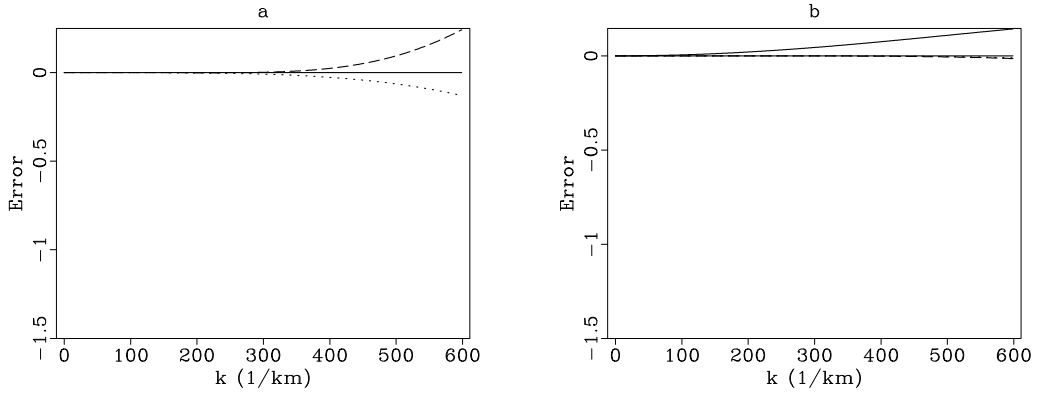

Figure 2: Errors for different approximations for $\cos(v(\mathbf{x})|\mathbf{k}|\Delta t) - 1$. Solid lines: exact solution ($\cos(v(\mathbf{x})|\mathbf{k}|\Delta t) - 1$) for $v = 4.0$ km/s and $v_0 = 2.0$ km/s. (a) Dash line: the 4th-order FD. Dotted line: pseudo-spectral method. (b) Dash line: the 2nd-order FFD method. Dotted line: the 4th-order FFD with v_0 as reference velocity. $\Delta t = 0.001$ s. $\Delta x = 0.005\, km$.

Δt). Namely,

$$\begin{aligned} q^{i,j,k}(t+\Delta t) = a^{i,j,k} q^{i,j,k}(t) \\ +b_1^{i,j,k}(q^{i-1,j,k}(t) + q^{i+1,j,k}(t)) \\ +b_2^{i,j,k}(q^{i,j-1,k}(t) + q^{i,j+1,k}(t)) \\ +b_3^{i,j,k}(q^{i,j,k-1}(t) + q^{i,j,k+1}(t)) \,, \end{aligned} \tag{9}$$

where i is the grid index of x_i direction;

5. $p(\mathbf{x}, t+\Delta t) \leftarrow q(\mathbf{x}, t+\Delta t) + 2p(\mathbf{x}, t) - p(\mathbf{x}, t-\Delta t)$.

Here $q(\mathbf{x}, t)$ and $\hat{q}(\mathbf{k}, t)$ are temporary functions.

The FFD approach is not limited to the isotropic case. In the case of transversally isotropic (TTI) media, the term $v(\mathbf{x})\,|\mathbf{k}|$ on the left-hand side of equation 7, can be replaced with the acoustic approximation (Alkhalifah, 1998, 2000; Fomel, 2004),

$$f(\mathbf{v}, \hat{\mathbf{k}}, \eta) = \sqrt{\frac{1}{2}(v_1^2\,\hat{k}_1^2 + v_2^2\,\hat{k}_2^2) + \frac{1}{2}\sqrt{(v_1^2\,\hat{k}_1^2 + v_2^2\,\hat{k}_2^2)^2 - \frac{8\eta}{1+2\eta} v_1^2 v_2^2\,\hat{k}_1^2\,\hat{k}_2^2}}\,, \tag{10}$$

where v_1 is the P-wave phase velocity in the symmetry plane, v_2 is the P-wave phase velocity in the direction normal to the symmetry plane, η is the anisotropic elastic parameter (Alkhalifah and Tsvankin, 1995) related to Thomsen's elastic parameters ϵ and δ (Thomsen, 1986) by

$$\frac{1+2\delta}{1+2\epsilon} = \frac{1}{1+2\eta}\,;$$

and $\hat{k}_1$ and $\hat{k}_2$ stand for the wavenumbers evaluated in a rotated coordinate system aligned with the symmetry axis:

$$\begin{aligned} \hat{k}_1 &= k_1 \cos\phi + k_2 \sin\phi \\ \hat{k}_2 &= -k_1 \sin\phi \cos\theta + k_2 \cos\phi \cos\theta + k_3 \sin\theta \\ \hat{k}_3 &= k_1 \sin\phi \sin\theta - k_2 \cos\phi \sin\theta + k_3 \cos\theta \ , \end{aligned} \tag{11}$$

where θ is the tilt angle measured with respect to vertical and ϕ is the angle between the projection of the symmetry axis in the horizontal plane and the original X-coordinate. The symmetry axis has the direction of $\{-\sin\theta\sin\phi, -\sin\theta\cos\phi, \cos\theta\}$.

Using these definitions, we develop a finite-difference approximation analogous to equation 7 for FFD in TTI media. The details of the derivation are given in the appendix. For the 2D TTI case, the corresponding FFD algorithm is as following:

1. Transform $p(\mathbf{x},t)$ to $\hat{p}(\mathbf{k},t)$ by FFT;
2. Multiply $\hat{p}(\mathbf{k},t)$ by $\dfrac{2[\cos(f(\mathbf{v_0},\hat{\mathbf{k}},\eta_0)\Delta t)-1]}{|\hat{\mathbf{k}}|^2}$ to get $\hat{q}(\mathbf{k},t)$;
3. Transform $\hat{q}(\mathbf{k},t)$ to $q(\mathbf{x},t)$ by inverse FFT;
4. Apply finite differences to $q(\mathbf{x},t)$ with coefficients in Table 1 to get $q(\mathbf{x},t+\Delta t)$. Namely,

$$\begin{aligned} q^{i,j,t+\Delta t} = {} & a^{i,j} q^{i,j,t} \\ & + b_1^{i,j}(q^{i-1,j,t} + q^{i+1,j,t}) \\ & + b_2^{i,j}(q^{i,j-1,t} + q^{i,j+1,t}) \\ & + d_1^{i,j}(q^{i-2,j,t} + q^{i+2,j,t}) \\ & + d_2^{i,j}(q^{i,j-2,t} + q^{i,j+2,t}) \\ & + c^{i,j}(q^{i-1,j-1,t} + q^{i-1,j+1,t} + q^{i+1,j-1,t} + q^{i+1,j+1,t}) \ . \end{aligned} \tag{12}$$

   where i is the grid index of x_i direction;
5. $p(\mathbf{x},t+\Delta t) \leftarrow q(\mathbf{x},t+\Delta t) + 2p(\mathbf{x},t) - p(\mathbf{x},t-\Delta t)$.

Here, $q(\mathbf{x},t)$ and $\hat{q}(\mathbf{k},t)$ are temporary functions.

NUMERICAL EXAMPLES

Our first example is a comparison of four methods: the 4th-order finite differences, pseudo-spectral method, velocity interpolation, and the FFD method in a velocity model with smooth variation, formulated as

$$v(x,z) \ = \ 550 + 1.5 \times 10^{-4}(x-800)^2 + 10^{-4}(z-500)^2;$$

$$0 \le x \le 2560,\ 0 \le z \le 2560.$$

The velocity is between 550 m/s and 1439 m/s. A Ricker-wavelet source with maximum frequency 70 Hz is located at the center of the model. For all the numerical simulations based on this model, we use the same grid size: $\Delta x = 5$ m and $\Delta t = 2$ ms.

Figure 3a shows an obvious numerical dispersion from the snapshot of the acoustic wavefield computed by the 4th-order finite difference method. Figure 3b shows a slight dispersion from the snapshot computed by pseudo-spectral method (Reshef et al., 1988b). Figure 3c shows the corresponding snapshot of the velocity-interpolation method (Etgen and Brandsberg-Dahl, 2009; Crawley et al., 2010), calculated using two reference velocities. It is practically free of dispersion thanks to spectral compensation. Figure 3d shows a snapshot of the proposed FFD method. It is almost exactly the same as Figure 3c; however, only one reference velocity is used instead of two. As comparison between Figure 3d and Figure 3c implies, the FFD method has practically the same accuracy as the velocity interpolation method while having only one reference velocity and therefore replacing the cost of one additional FFT with the cost of a low-order finite-difference operator.

Our next example is a snapshot of the acoustic wavefield calculated by FFD in the BP model (Billette and Brandsberg-Dahl, 2004). We use a Ricker-wavelet at a point source. The maximum frequency is 50 Hz. The horizontal grid size Δx is 37.5 m, the vertical grid size Δz is 12.5 m and the time step is 1 ms. Figure 4 shows a part of the model with a salt body. Figure 5 shows a wavefield snapshot confirming that the FFD method can work in a complex-velocity medium as well.

Next we apply our FFD algorithm to RTM with a simple exponential decaying boundary condition (Cerjan et al., 1985). The dominant frequency is 27 Hz. The space grid is 25 m and the time step is 1.5 ms. Figure 6 shows the output image. The inner and outer flanks of the salt body are clearly imaged.

The cost advantage of FFD is even more appealing in anisotropic (TTI) media, which require multiple velocity parameters and increase the cost of velocity interpolation. Figure 7 shows the impulse response of a 4th-order FFD operator in a TTI model with the tilt of 45° and a smooth velocity variation (v_x: 800-1225.41 m/s, v_z: 700-883.6 m/s). The space grid size is 5 m and the time step is 1 ms. Note no coupling of qP-waves and qSV-waves (Zhang et al., 2009) in the figure, thanks to the Fourier construction of the operator.

For this paper, we implemented a 2nd-order 5-point FD scheme for 2D isotropic case. One can observe little dispersion in isotropic examples. For TTI media, we use a 13-point scheme which minimizes the error in the symmetry plane and in the direction normal to the symmetry plane. One can still see some dispersion in the corresponding snapshot; which indicates that a higher order FD scheme might be

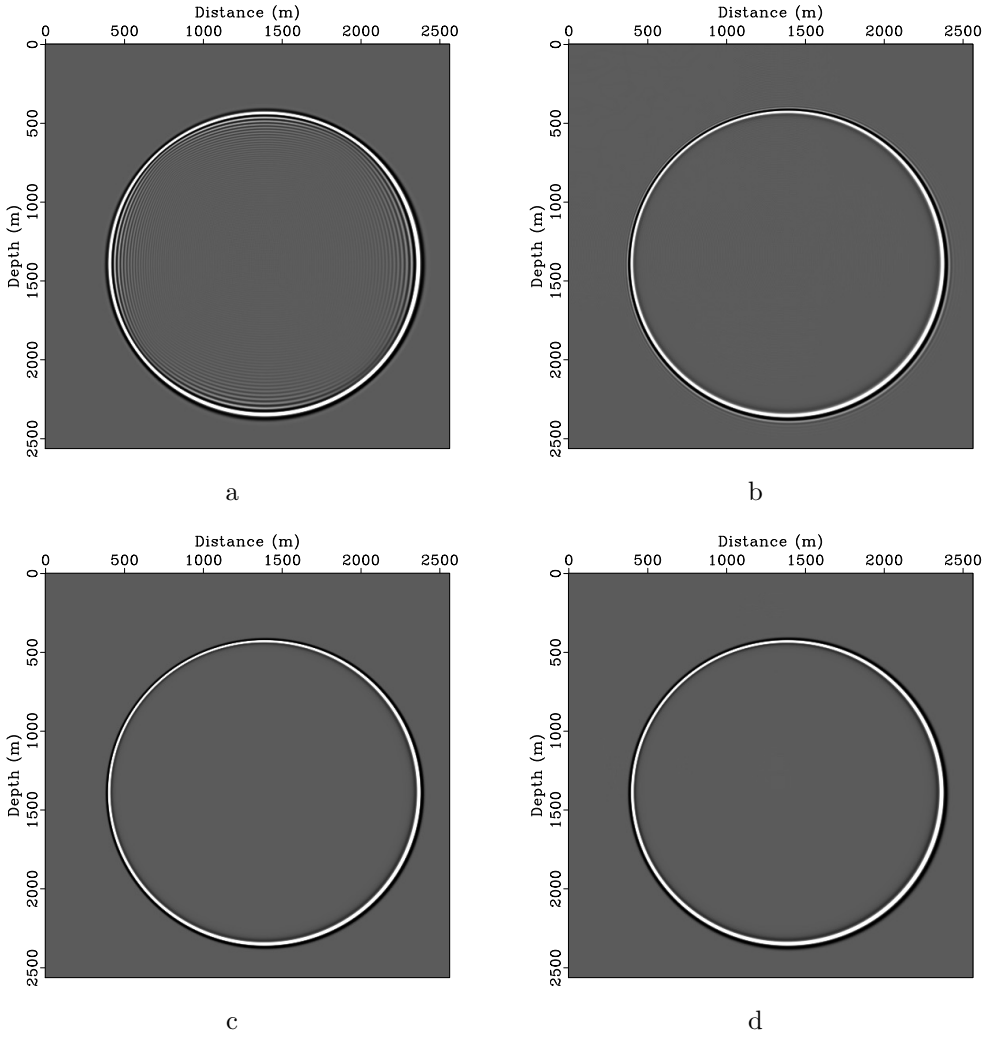

Figure 3: Acoustic wavefield snapshot by: (a) 4th-order Finite Difference method; (b) pseudo-spectral method; (c) velocity interpolation method with 2 reference velocities; (d) FFD method with RMS velocity.

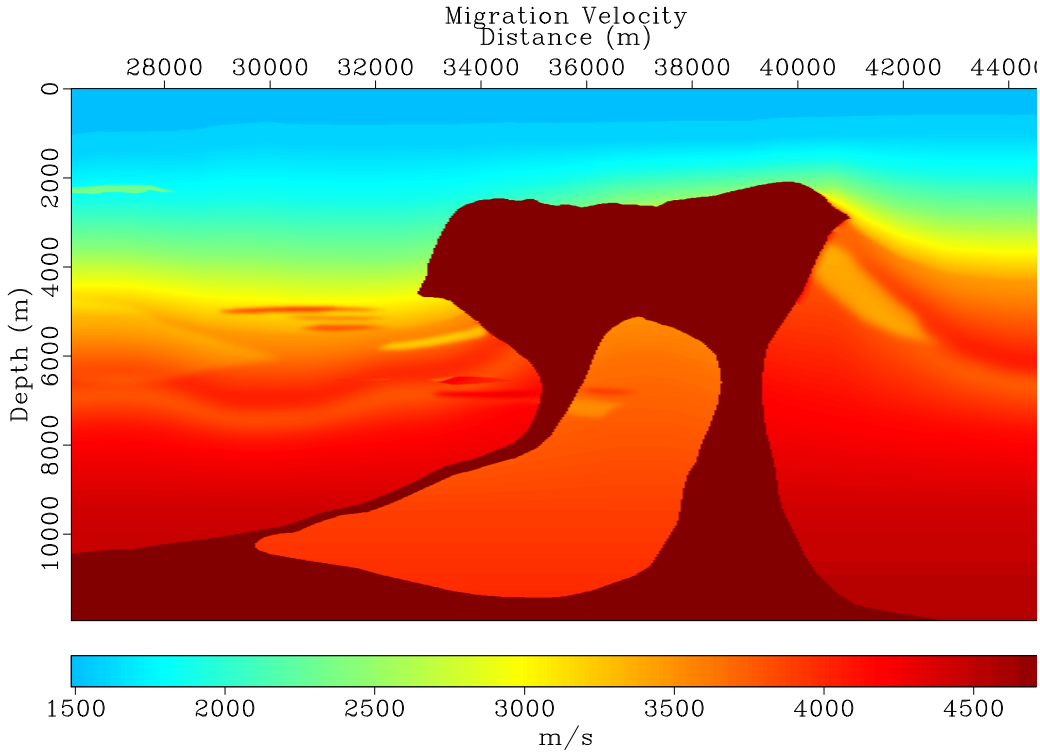

Figure 4: Portion of BP 2004 synthetic velocity model.

required to further supress the dispersion.

Our last example is qP-wave simulation in the BP 2D TTI model. Figure 8a-8d shows parameters for part of the model. The maximum frequency is 50 Hz. The space grid size is 12.5 m and the time step is 1 ms. The snapshot of the acoustic wavefield in Figure 9 demonstrates the stability of our approach in a complicated anisotropic model. Some small dispersion is present in the TTI examples, pointing to a possible need to extend the FD part of the FFD scheme from second order to higher orders.

CONCLUSIONS

Accurate and efficient numerical wave propagation in variable velocity media is crucial for seismic modeling and seismic migration, particularly for reverse-time migration. The FFD technique proposed in this paper promises higher accuracy than that of the conventional, explicit finite-difference method, at the cost of only one forward and inverse Fast Fourier Transform. Results in synthetic isotropic and anisotropic models illustrate FFD's stability in complicated velocity models. The method can be used in reverse-time migration to enhance its accuracy and stability.

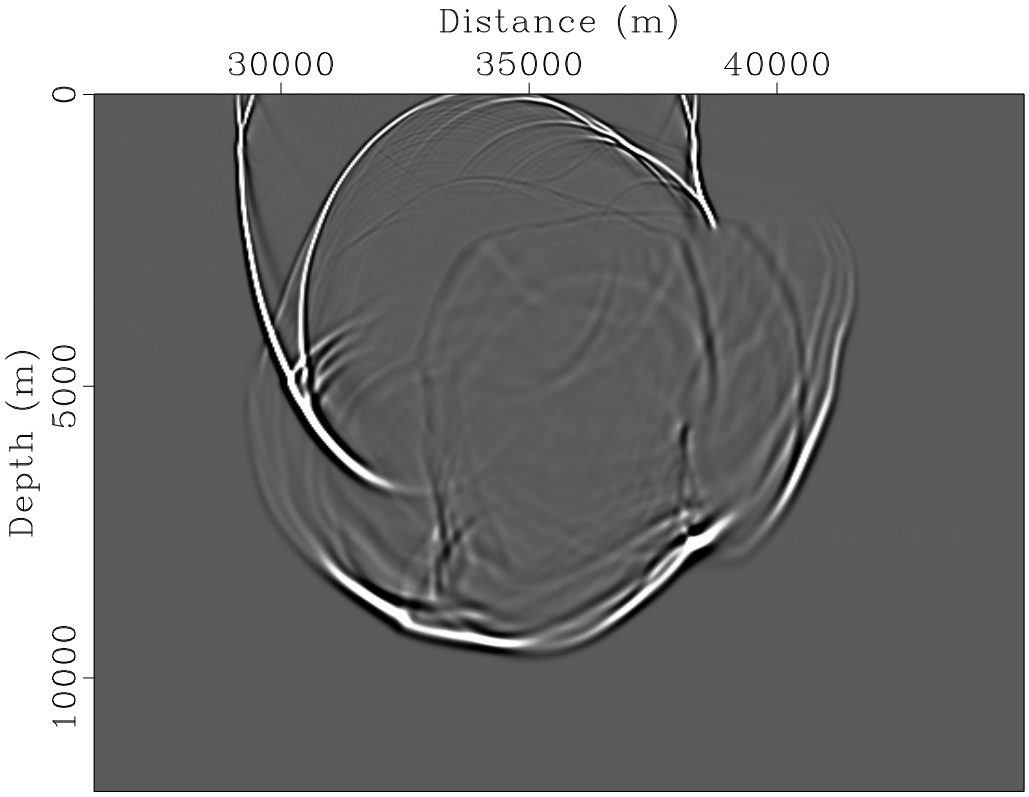

Figure 5: Wavefield snapshot in the BP Model shown in Figure 4.

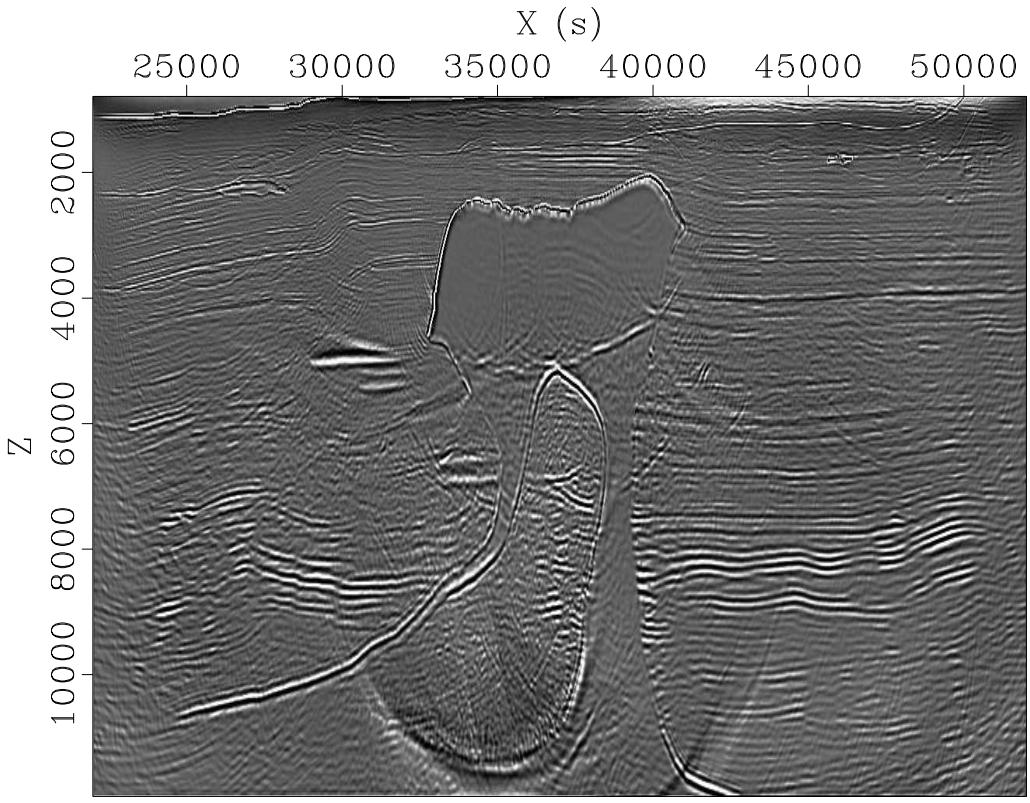

Figure 6: RTM image of BP salt model.

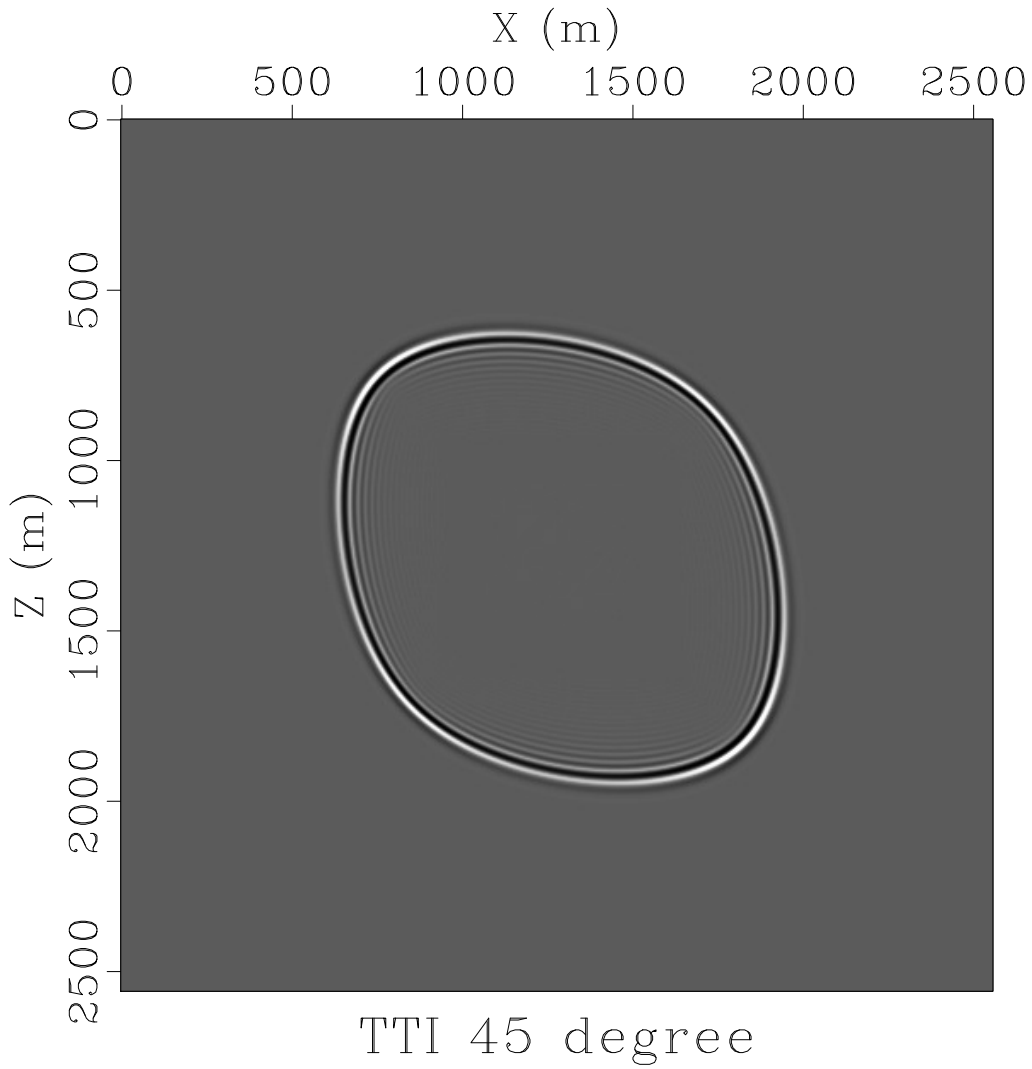

Figure 7: Wavefield snapshot in a TTI medium with tilt of 45 degrees. $v_x(x,z) = 800 + 10^{-4}(x-1000)^2 + 10^{-4}(z-1200)^2$; $v_z(x,z) = 700 + 10^{-4}(z-1200)^2$; $\eta = 0.3$; $\theta = 45^\circ$.

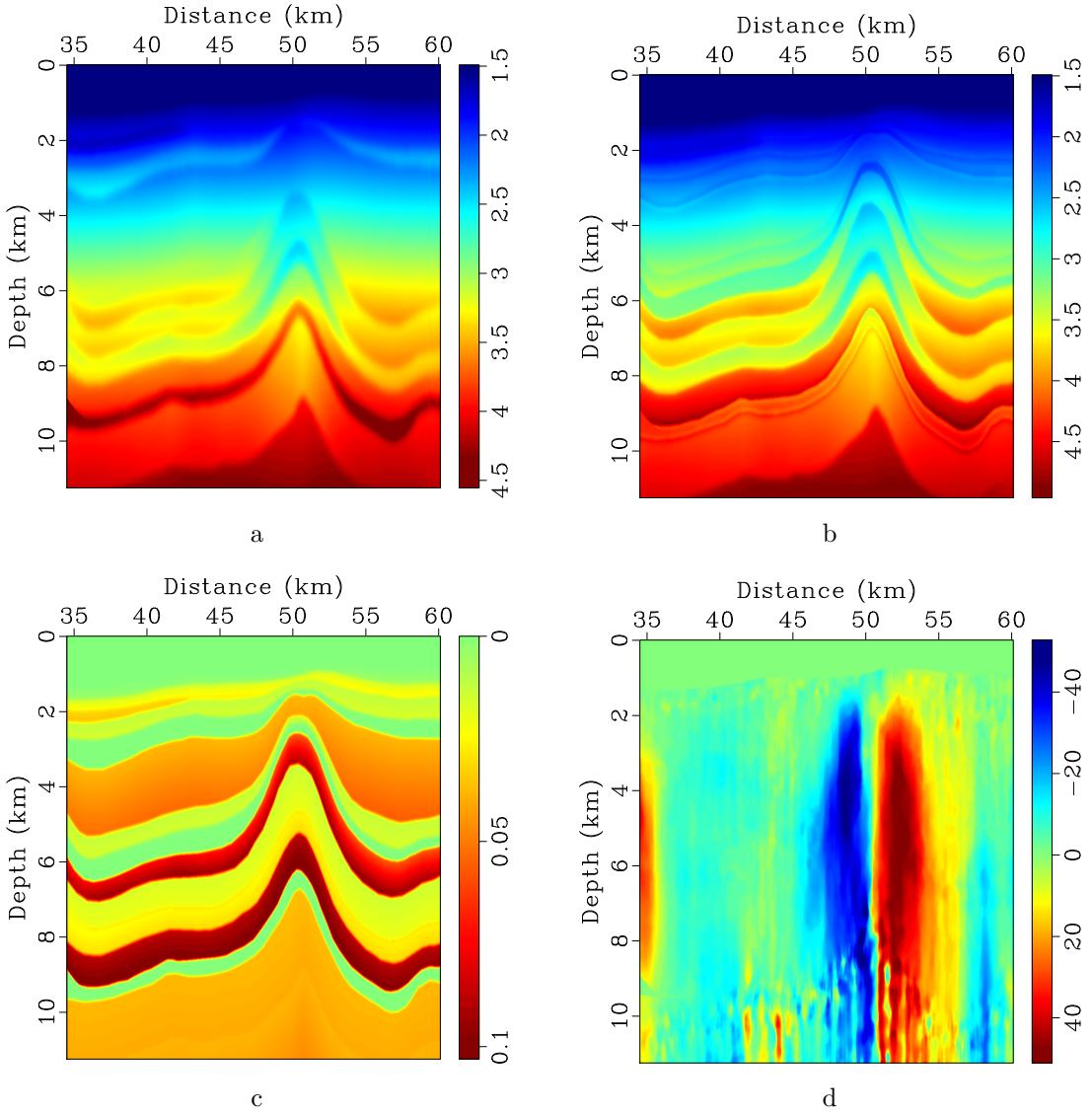

Figure 8: Partial region of the 2D BP TTI model. a: v_z. b: v_x. c: η. d:θ.

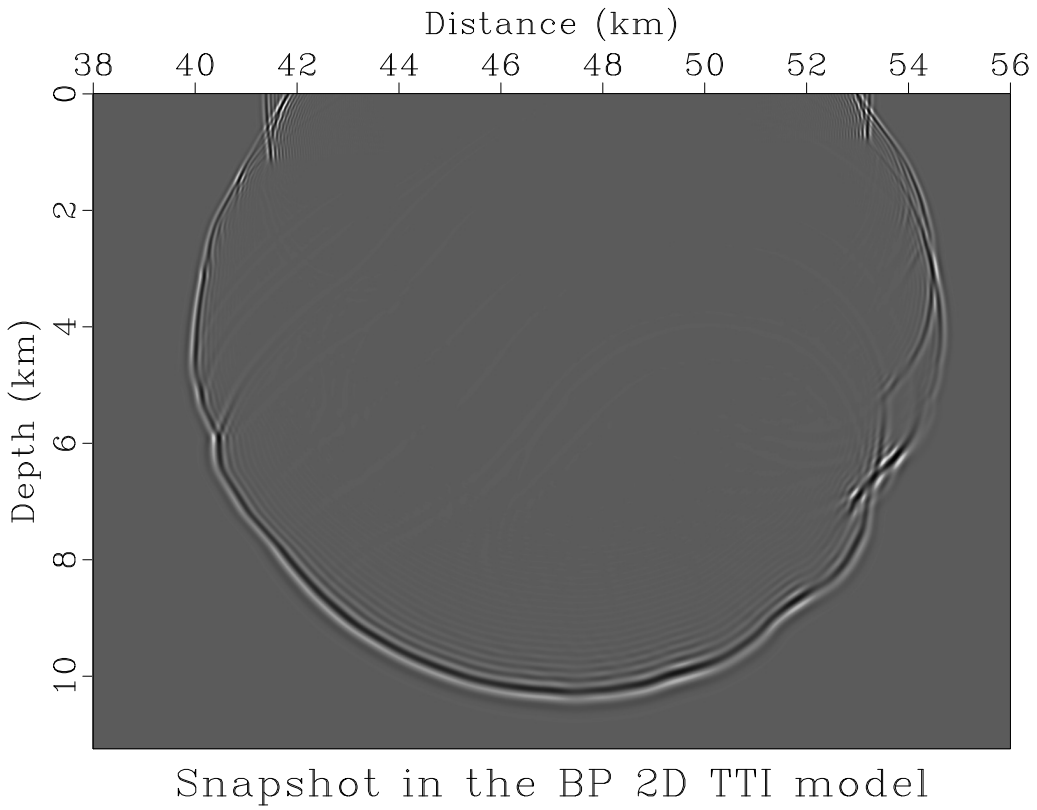

Figure 9: Scalar wavefield snapshot in the 2D BP TTI model, shown in Figure 8.

ACKNOWLEDGEMENT

We thank BP for releasing benchmark synthetic models, Bjorn Enquist, Paul Fowler and Lexing Ying for useful discussions, and John Etgen, Stig Hestholm, Erik Saenger and two anonymous reviewers for helpful reviews.

This publication is authorized by the Director, Bureau of Economic Geology, The University of Texas at Austin.

APPENDIX A

FFD FOR TTI MEDIA

To develop a 25-point finite-difference scheme analogous to equation 7 for FFD in 3D TTI media, we first apply the following approximation:

$$\begin{aligned}\frac{\cos(f(\mathbf{v},\hat{\mathbf{k}},\eta)\Delta t)-1}{\cos(f(\mathbf{v_0},\hat{\mathbf{k_0}},\eta_0)\Delta t)-1}|\hat{\mathbf{k}}|^2 \approx \\ a+2\sum_{n=1}^{3}\left(b_n\cos(k_n\Delta x_n)+d_n\cos(2k_n\Delta x_n)\right) \\ +2\sum_{n=1}^{3}c_n[\cos(k_i\Delta x_i+k_j\Delta x_j)+\cos(k_i\Delta x_i-k_j\Delta x_j)]\ ,\end{aligned} \tag{A-1}$$

where $i,j=1,2,3$; $i\neq j$; $i,j\neq n$.

In approximation A-1, $f(\mathbf{v},\hat{\mathbf{k}},\eta)$ is a function as in expression 10 and a, b_n, c_n and d_n are coefficients determined from the Taylor expansion around $k=0$.

Notice that we multiply the left-hand side with $|\hat{\mathbf{k}}|^2$, so one needs to multiply $\hat{p}(\hat{\mathbf{k}},\mathbf{t})$ with $\dfrac{2[\cos(f(\mathbf{v_0},\mathbf{k},\eta_0)\Delta t)-1]}{|\hat{\mathbf{k}}|^2}$.

The coefficients for Equation A-1 are derived in Table 1 and Table 2. w_{n0}, h_{n0}, p_{n0} and q_{n0} have similar expressions as above in Table 2 with $\mathbf{v}$, η and θ substited by the corresponding reference values: RMS velocity $\mathbf{v}_0$, average anisotropic parameter η_0 and average tilt angles θ_0 and ϕ_0.

REFERENCES

Alkhalifah, T., 1998, Acoustic approximations for processing in transversely isotropic media: Geophysics, **63**, 623–631.

———, 2000, Acoustic approximations for processing in transversely isotropic media: Geophysics, **65**, 1239–1250.

Alkhalifah, T., and I. Tsvankin, 1995, Velocity analysis for transversely isotropic media: Geophysics, **60**, 1550–1566.

Baysal, E., D. D. Kosloff, and J. W. C. Sherwood, 1983, Reverse time migration: Geophysics, **48**, 1514–1524.

a	$a = -2b_1 - 2b_2 - 2b_3 - 4c_1 - 4c_2 - 4c_3 - 2d_1 - 2d_2 - 2d_3$
b	$b_1 = -2c_2 - 2c_3 - 4d_1 - \dfrac{w_1 + h_1}{\Delta x_1^2 (w_{10} + h_{10})}$
c	$b_2 = -2c_1 - 2c_3 - 4d_2 - \dfrac{w_2 + h_2}{\Delta x_2^2 (w_{20} + h_{20})}$
d	$b_3 = -2c_1 - 2c_2 - 4d_3 - \dfrac{w_3 + h_3}{\Delta x_3^2 (w_{30} + h_{30})}$
e	$d_1 = \dfrac{(w_1 + h_1)(2x_1^2 + \Delta t^2 (w_{10} + h_{10} - w_1 - h_1))}{24 \Delta x_1^4 (w_{10} + h_{10})}$
f	$d_2 = \dfrac{(w_2 + h_2)(2x_2^2 + \Delta t^2 (w_{20} + h_{20} - w_2 - h_2))}{24 \Delta x_2^4 (w_{20} + h_{20})}$
g	$d_3 = \dfrac{(w_3 + h_3)(2x_3^2 + \Delta t^2 (w_{30} + h_{30} - w_3 - h_3))}{24 \Delta x_3^4 (w_{30} + h_{30})}$
h	$c_1 = \dfrac{1}{12 \Delta x_2^2 \Delta x_3^2} \left[\dfrac{\Delta x_2^2 (w_2 + h_2)}{w_{20} + h_{20}} + \dfrac{\Delta x_3^2 (w_3 + h_3)}{w_{30} + h_{30}} \right] - d_2 \dfrac{\Delta x_2^2}{\Delta x_3^2} - d_3 \dfrac{\Delta x_3^2}{\Delta x_2^2} + \dfrac{\Delta t^2 (p_1 + q_1)(p_1 0 + q_1 0 - p1 - q1)}{12 \Delta x_2^2 \Delta x_3^2 (p_1 0 + q_1 0)}$
i	$c_2 = \dfrac{1}{12 \Delta x_1^2 \Delta x_3^2} \left[\dfrac{\Delta x_1^2 (w_1 + h_1)}{w_{10} + h_{10}} + \dfrac{\Delta x_3^2 (w_3 + h_3)}{w_{30} + h_{30}} \right] - d_1 \dfrac{\Delta x_1^2}{\Delta x_3^2} - d_3 \dfrac{\Delta x_3^2}{\Delta x_1^2} + \dfrac{\Delta t^2 (p_2 + q_2)(p_2 0 + q_2 0 - p2 - q2)}{12 \Delta x_1^2 \Delta x_3^2 (p_2 0 + q_2 0)}$
j	$c_3 = \dfrac{1}{12 \Delta x_1^2 \Delta x_2^2} \left[\dfrac{\Delta x_1^2 (w_1 + h_1)}{w_{10} + h_{10}} + \dfrac{\Delta x_2^2 (w_2 + h_2)}{w_{20} + h_{20}} \right] - d_1 \dfrac{\Delta x_1^2}{\Delta x_2^2} - d_2 \dfrac{\Delta x_2^2}{\Delta x_1^2} + \dfrac{\Delta t^2 (p_3 + q_3)(p_3 0 + q_3 0 - p3 - q3)}{12 \Delta x_1^2 \Delta x_2^2 (p_3 0 + q_3 0)}$

Table 1: Coefficients for equation A-1.

a	$w_1 = v_1^2 \cos^2\phi + \sin^2\phi(v_1^2\cos^2\theta + v_2^2\sin^2\theta)$
b	$w_2 = (v_1^2 + v_2^2)\cos^2\phi\cos^2\theta + v_1^2\sin^2\theta$
c	$w_3 = v_1^2\sin^2\theta + v_2^2\cos^2\theta$
d	$h_1 = \sqrt{w1^2 - \dfrac{8\eta v_1^2 v_2^2 \sin^2\phi(\cos^2\phi + \sin^2\phi\cos^2\theta)\sin^2\theta}{1+2\eta}}$
e	$h_2 = \sqrt{w2^2 - \dfrac{8\eta v_1^2 v_2^2 \cos^2\phi\cos^2\theta(\cos^2\phi\cos^2\theta + \sin^2\phi)}{1+2\eta}}$
f	$h_3 = \sqrt{w3^2 - \dfrac{8\eta v_1^2 v_2^2 \cos^2\theta\sin^2\theta}{1+2\eta}}$
g	$p_1 = w_2 + w_3 + v_1^2\cos\phi\sin 2\theta - 2v_2^2\cos\phi\cos^2\theta$
h	$q_1 = \sqrt{p_1^2 - \dfrac{32\eta v_1^2 v_2^2 \cos^2\theta\sin^4\frac{\phi}{2}(\cos^2\phi\cos^2\theta + \sin^2\theta + \sin^2\phi + \cos\phi\sin 2\theta)}{1+2\eta}}$
i	$p_2 = w_1 + w_3 + (v_2^2 - v_1^2)\sin\phi\sin 2\theta$
j	$q_2 = \sqrt{p_2^2 - \dfrac{8\eta v_1^2 v_2^2(\cos\theta + \sin\phi\sin\theta)^2(\cos^2\phi + (\cos\theta\sin\phi - \sin\theta)^2)}{1+2\eta}}$
k	$p_3 = w_1 + w_2 + v_1^2\sin^2\theta\sin 2\phi + \frac{1}{2}v_2^2\sin 2\phi\sin 2\theta$
l	$q_3 = \sqrt{p_3^2 - \dfrac{4\eta v_1^2 v_2^2\cos^2(\phi+\theta)(\sin 2\phi\cos 2\theta - 3 - \cos 2\theta - \sin 2\phi)}{1+2\eta}}$

Table 2: Coefficients for Table 1.

Bednar, J., 2005, A brief history of seismic migration: Geophysics, **70**, 3MJ–20MJ.

Billette, F. J., and S. Brandsberg-Dahl, 2004, The 2004 BP velocity benchmark: 67th Annual EAGE Meeting, EAGE, Expanded Abstracts, B305.

Cerjan, C., D. Kosloff, R. Kosloff, and M. Reshef, 1985, A nonreflecting boundary condition for discrete acoustic and elastic wave equations: Geophysics, **50**, 705–708.

Crawley, S., S. Brandsberg-Dahl, and J. McClean, 2010, 3d TTI RTM using the pseudo-analytic method: 80th Ann. Internat. Mtg., Soc. Expl. Geophys., 3216–3220.

Du, X., R. P. Fletcher, and P. J. Fowler, 2010, Pure P-wave propagators versus pseudo-acoustic propagators for RTM in VTI meida: 72nd Annual EAGE Meeting, EAGE, Expanded Abstracts, Accepted.

Etgen, J., 1989, Accurate wave equation modeling, *in* SEP-60: Stanford Exploration Project, 131–148.

Etgen, J., and S. Brandsberg-Dahl, 2009, The pseudo-analytical method: application of pseudo-Laplacians to acoustic and acoustic anisotropic wave propagation: 79nd Annual International Meeting, SEG, Expanded Abstracts, 2552–2556.

Etgen, J., S. H. Gray, and Y. Zhang, 2009, An overview of depth imaging in exploration geophysics: Geophysics, **74**, WCA5–WCA17.

Fletcher, R. P., X. Du, and P. J. Fowler, 2009, Reverse time migration in tilted transversely isotropic (TTI) media: Geophysics, **74**, WCA179–WCA187.

Fomel, S., 2004, On anelliptic approximations for qP velocities in VTI media: Geophysical Prospecting, **52**, 247–259.

Fomel, S., L. Ying, and X. Song, 2010, Seismic wave extrapolation using a lowrank symbol approximation: 80th Ann. Internat. Mtg., Soc. Expl. Geophys., 3092–3096.

Fowler, P. J., X. Du, and R. P. Fletcher, 2010, Coupled equations for reverse time migration in transversely isotropic media: Geophysics, **75**, S11–S22.

Levin, S. A., 1984, Principle of reverse time migration: Geophysics, **49**, 581–583.

Liu, F., S. A. Morton, S. Jiang, L. Ni, and J. P. Leveille, 2009, Decoupled wave equations for P and SV waves in an acoustic VTI media: 79th Ann. Internat. Mtg., Soc. Expl. Geophys., 2844–2848.

Liu, Y., and M. K. Sen, 2009, A new time-space domain high-order finite-difference method for the acoustic wave equation: Journal of computational Physics, **228**, 8779–8806.

McMechan, G. A., 1983, Migration by extrapolation of time-dependent boundary values: Geophys. Prosp., **31**, 413–420.

Pestana, R. C., and P. L. Stoffa, 2010, Time evolution of the wave equation using rapid expansion method: Geophysics, **75**, T121–T131.

Reshef, M., D. Kosloff, M. Edwards, and C. Hsiung, 1988a, Three-dimensional acoustic modeling by the Fourier method: Geophysics, **53**, 1175–1183.

———, 1988b, Three-dimensional acoustic modeling by the fourier method: Geophysics, **53**, 1175–1183.

Ristow, D., and T. Ruhl, 1994, Fourier finite-difference migration: Geophysics, **59**, 1882–1893.

Song, J., 2001, The optimized expression of a high dimensional function/manifold in a lower dimensional space: Chinese Scientific Bulletin, **46**, 977–984.

Soubaras, R., and Y. Zhang, 2008, Two-step explicit marching method for reverse time migration: 78th Ann. Internat. Mtg., Soc. Expl. Geophys., 2272–2276.

Symes, W. W., 2007, Reverse time migration with optimal checkpointing: Geophysics, **72**, SM213–SM221.

Tal-Ezer, H., D. Kosloff, and Z. Koren, 1987, An accurate scheme for seismic forward modeling: Geophysical Prosecting, **35**, 479–490.

Thomsen, L., 1986, Weak elastic anisotropy: Geophysics, **51**, 1954–1966.

Whitmore, N. D., 1983, Iterative depth migration by backward time propagation: 53rd Ann. Internat. Mtg., Soc. Expl. Geophys., 382–385.

Wu, W., L. R. Lines, and H. Lu, 1996, Analysis of high-order, finite-difference schemes in 3-D reverse-time migration: Geophysics, **61**, 845–856.

Yoon, K., K. J. Marfurt, and W. Starr, 2004, Challenges in reverse-time migration: 74th Ann. Internat. Mtg., Soc. Expl. Geophys., 1057–1061.

Zhang, H., G. Zhang, and Y. Zhang, 2009, Removing S-wave noise in TTI reverse time migration: 79th Ann. Internat. Mtg., Soc. Expl. Geophys., 2849–2853.

Zhang, Y., and G. Zhang, 2009, One-step extrapolation method for reverse time migration: Geophysics, **74**, A29–A33.